Batteries & Supercaps

Research Article
doi.org/10.1002/batt.202400693

Chemistry Europe
European Chemical Societies Publishing

www.batteries-supercaps.org

On the Description of Electrode Materials in Lithium Ion Batteries Based on the Quantification of Work Functions

Johanna Schepp,[a] Jona Schuch,[b] Jan P. Hofmann,*[b] and Karl-Michael Weitzel*[a]

During charging of a lithium ion battery, electrons are transferred from the cathode material to the outer circuit and lithium ions are transferred into the electrolyte. Here, the energy required to take electrons and lithium ions out of two prototypical cathode materials, Li_xFePO_4 and $Li_xMn_2O_4$ is investigated as a function of the state of lithiation, x. Both electronic and ionic work functions vary significantly with x for Li_xFePO_4 but rather little for $Li_xMn_2O_4$. The relevance of these work functions for the thermodynamic description of lithium ion batteries is discussed.

1. Introduction

Lithium ion batteries (LIBs) are an important part of today's daily live, being used in many different applications such as mobile computers, electro-mobility or energy storage.[1, 2,3,4,5] One of the most important properties of LIBs is the open circuit voltage (OCV), i.e., the voltage measured across a device for zero current. According to the standard notation, the OCV of a LIB is described by (1)[6,7,8]

$$OCV = \frac{\mu(Li)_C - \mu(Li)_A}{e} \quad (1)$$

where $\mu(Li)_C$ and $\mu(Li)_A$ are the chemical potentials of lithium in the cathode (C) and the anode (A), e represents the elementary charge. Often, the chemical potential of the lithium in the electrodes is set equal to the chemical potential of the electrons, $\mu(e^-)$, in these electrodes leading to (2)[9]

$$OCV = \frac{\mu(e^-)_C - \mu(e^-)_A}{e} \quad (2)$$

The chemical potentials of the electrons is identified as the electronic Fermi level, $E_F(e^-)$, which correlates with the electronic work function. This leads to the commonly presented result that the OCV can be identified with the difference of the electronic work functions $w(e^-)$ of the electrode material.

$$OCV = E_F(e^-)_C - E_F(e^-)_A = w(e^-)_C - w(e^-)_A \quad (3)$$

As pointed out by Bruce this should be considered an approximation.[10] The above-mentioned concept is based on the assumption of equilibrium between lithium atoms and the corresponding lithium ion and electron, $\mu(Li) = \mu(Li^+) + \mu(e^-)$ and subsequently setting $\mu(Li^+)_C - \mu(Li^+)_A = 0$. This is equivalent to neglecting ionic contributions to the balance of the chemical potentials in the LIB and can only be regarded an approximation.[10]

On the other hand, in a seminal paper, Gerischer argued that the thermodynamic description of the exchange of ions and electrons in a battery material during charging and discharging should be described using the ionic and electronic contributions to this process.[11] In more detail, the total Gibbs energy of a battery ΔG_{tot} can be divided into the ionic (ΔG_{ion}) and electronic (ΔG_{el}) contributions and using this, the cell voltage ($-e \cdot \Delta U$) of a battery system can be described by

$$\Delta G_{tot} = \Delta G_{el} + \Delta G_{ion} = -e \cdot \Delta U \quad (4)$$

In the language of the OCV formalism, this would lead to

$$OCV = \frac{(\mu(Li^+)_C + \mu(e^-)_C) - ((\mu(Li^+)_A + \mu(e^-)_A)}{e} \quad (5)$$

In analogy to the common practice for describing electrons, we propose to identify the chemical potential of the lithium ions with the corresponding ionic Fermi energy. The concept of the ionic Fermi energy has been elaborated in the context of ion transport in potential energy landscapes.[12,13] The importance of ionic site energies for LIBs has already been pointed out by Bruce.[10] When referenced to the vacuum level – these ionic Fermi energies can be translated to the corresponding ionic work functions. This leads to Eq. (6)

[a] J. Schepp, K.-M. Weitzel
Philipps-Universität Marburg, Chemistry Department, 35032 Marburg, Germany
E-mail: weitzel@chemie.uni-marburg.de

[b] J. Schuch, J. P. Hofmann
Surface Science Laboratory, Department of Materials- and Geosciences, Technical University of Darmstadt, Peter-Grünberg-Straße 4, 64287 Darmstadt, Germany
E-mail: hofmann@surface.tu-darmstadt.de

Supporting information for this article is available on the WWW under https://doi.org/10.1002/batt.202400693

$$OCV = (E_F(Li^+)_C + E_F(e^-)_C) - (E_F(Li^+)_A + E_F(e^-)_A) = (w(Li^+)_C + w(e^-)_C) - (w(Li^+)_A + w(e^-)_A) \quad (6)$$

Equation (6) can be represented in the form of a Born cycle, where the sum of the work functions on the right side (with correct sign) yields the theoretical OCV. Such Born cycles will be discussed in this work for typical electrode materials in LIBs.

One example of a Born cycle describing the open cell voltage of the Li/$LiCoO_2$ battery system has been reported by Schuld et al.[14] That cycle takes into account the ionic ($w(Li^+)$) and electronic ($w(e^-)$) work functions of $LiCoO_2$ as well as literature values for the ionization energy of lithium atoms in the gas phase ($IE(Li)$) and the sublimation enthalpy of lithium atoms from metallic lithium ($\Delta H_{subl}(Li)$).

$$e \cdot \Delta U_{cell} = w(Li^+)_{LCO} + w(e^-)_{LCO} - IE(Li) - \Delta H_{subl}(Li) \quad (7)$$

The open cell voltage estimated using that approach approximately matched literature values for the open cell voltage of the system. However, that work only compared the work functions of fully lithiated lithium cobalt oxide and the agreement between measured OCV and OCV estimated based on Eq. (7) may be fortuitous. A variation of the state of lithiation was not considered. The concept of Born cycles in the discussion of thermodynamic properties of LIBs has also been pursued by Qi and coworkers.[15] Born cycles involving ionic and electronic work functions have further been established for describing metal dissolution and corrosion potential.[16]

In the present work, the ionic and electronic work functions of Li_xFePO_4 and $Li_xMn_2O_4$ – two prototypical cathode materials in LIBs – are measured experimentally as function of the degree of lithiation/delithiation.

In principle equation (6) describes the theoretical potential difference between a cathode material and an anode material. So does Eq. (1) and (2). As such, these equations apply to the separate electrode materials only. As we will show below, neither equation (3) nor equation (6) is capable of reproducing the experimentally measured OCV for the examples discussed. As a consequence, for a complete thermodynamic cycle applying to a realistic LIB, and thus predicting a realistic OCV, one has to invoke additional terms in the energy balance, e.g., the solvation energies of ions and voltage drops across interfacial zones. This will be elaborated at a later point.

1.1. Introduction to Structural and Energetic Properties of the $LiFePO_4$ System

The lithium iron phosphate system is one of the cathode materials with wide spread commercial use.[17] Since the report by Padhi,[18] the interest in the perspective of $LiFePO_4$ as a cathode material has risen sharply.[19,20,21,22] The wide field of $LiFePO_4$ related scientific reports includes structure, morphology, phase segregation, transport, and other general electrochemistry investigations. $LiFePO_4$ is a naturally existing mineral with the name triphylite. It belongs to the olivine family of minerals crystallizing in the orthorhombic lattice structure in the space group Pnma.[23] The crystal structure may be visualized by a combination of corner-shared FeO_6 octahedra and edge-share LiO_6 octahedra. Extraction of Li during delithiation ultimately leads to $FePO_4$ retaining the olivine framework, however with considerable distortion.[24] Transport in the pure $LiFePO_4$ phase is dominant along the b-axis of the unit cell.[25] During delithiation, the transport characteristics is altered significantly including a change to multi dimensionality.[26] The latter is connected to the complexity of the phase diagram of the $Li_xFePO_4/FePO_4$ system relevant for discussing delithiation. In brief, below 200 °C, Li_xFePO_4 is dominated by a mixture of triphylite $LiFePO_4$ and heterosite $FePO_4$ in a ratio given by the amount of lithium present. Above 300 °C, a disordered solid solution of Li_xFePO_4 dominates.[27] Between 200 °C and 300 °C, mixtures of this disordered solid solution with either the triphylite or the heterosite phase are observed. On the other hand, segregation into Li rich and Li poor regions has been questioned by Bazant and coworkers.[28] The complexity of the situation is further increased by the fact that the memory of a given sample depends on specific details of material processing and may correspond to a thermodynamic equilibrium but may also correspond to a metastable state. Values regarding the partial ionic and electronic conductivity of $LiFePO_4$ appear to exhibit considerable uncertainty. Early work by Amin et al. reported the electronic conductivity to be much higher than the ionic conductivity.[29] Later work by Ohmer reported the opposite relation.[30]

1.2. Introduction to the Structural and Energetic Properties of the $LiMn_2O_4$ System

$LiMn_2O_4$ is another candidate for high performance cathodes in LIBs.[31] $LiMn_2O_4$ crystallizes in the cubic spinel structure with space group Fd3m.[32] Here, the lithium occupies the tetrahedral site and Mn the octahedral sites of the cubic face centered oxygen network. Complete delithiation leads to MnO_2. The delithiation by removal of lithium from the tetrahedral sites is believed to occur sequentially in steps associated with two plateaus in the voltage capacity diagrams.[33] These plateaus are sometimes discussed as reflecting different coexisting phases, however, for all values of $0 \leq x \leq 1$ in $Li_xMn_2O_4$, the structure remains cubic and the lattice parameters evolve smoothly. [34] A pronounced two phase region has been predicted for the range of $1 \leq x \leq 2$, i.e., a lithiated $LiMn_2O_4$.[35] That range of composition will not be further discussed in this work. The partial ionic and electronic transport coefficients are again subject of some dispute. Even for the total electrical conductivity, numbers reported range from 10^{-6} to 10^{-4} S/cm at room temperature. The ionic conductivity was reported to be larger than the electronic conductivity.[36] From fitting experimental impedance spectroscopy data, Zhuang et al. concluded that the ionic conductivity is not discernible and the total conductivity is basically assigned to the electronic conductivity.[37]

Research Article
doi.org/10.1002/batt.202400693
Chemistry Europe
European Chemical Societies Publishing

1.3. Concept of Work Function Measurements by Thermionic Emission and Photoelectron Spectroscopy

The goal of the current work is to contribute to a better understanding of the thermodynamic properties of the two prototypical LIB cathode materials, $LiFePO_4$ and $LiMn_2O_4$, by studying the ionic and the electronic work functions as a function of the state of lithiation/delithiation. Since charging and decharging of a lithium ion battery is associated with taking electrons and lithium ions out of a LIB cathode (or bring into it), it appears interesting to study how much energy is required to take an electron or a lithium ion out of a cathode material and transfer it to the current collector and the electrolyte, respectively. This constitutes the relevance of transfer energies. As of today, there are no known concepts of measuring these transfer energies in a complete cell. The full cell, albeit clearly the technical device of relevance, contains too many components and – even more problematic – too many ill-defined interfaces. Thus, for advancing the fundamental understanding of the charge transfer processes in ion batteries, it appears rewarding to break down and simplify the problem into tractable parts. Here, we decide to literally focus the attention to the energy required for taking an electron and a lithium ion out of a LIB cathode material. This energy is considered to be an essential part of the technically relevant cell potential, although likely not the only constituent. Conceptually, the energy required to take a charged particle out of a macroscopic solid and bring it to infinite distance from the solid sample in vacuum is defined as the *work function*.

There are two established techniques for determining work functions for ions and electrons. One technique for measuring work functions is the thermionic emission.[38] Pioneered by O. W. Richardson, thermionic emission refers to the emission of "electricity" by a hot body placed into an electric field. The process is applicable to both the emission of electrons and of ions from a solid body. More specifically, thermionic emission can be divided in three different regimes depending on the electric field applied to the measured sample.[39] For small electric fields, the emission current can be described by the Child-Langmuir model.[40,41] In this regime, the emission current is limited as a space charge zone forms in front of the emitter. For high electric fields, the emission current is increased as the effective work function of the sample is decreased. This effect is described by the Schottky model.[42] The thermionic measurements described in this work were performed in the Richardson-Dushman regime, which lies in between the before mentioned regimes.[43] In this regime, the emission current is effectively independent of the applied electric field but strongly varies with the temperature of the emitter. The emission current in the Richardson-Dushman regime, I_{RD}, can be described as:

$$I_{RD} = A_R \cdot T^2 \cdot exp\left(-\frac{w}{k_B \cdot T}\right) \tag{8}$$

where w is the electronic or ionic work function and A_R is an empirical constant. For some of the samples, the thermionic emission current slowly decays with time, due to insufficient charge compensation. In that case the equation (8) is complemented by a simple mono-exponential decay function of the kind $\exp(-t/\tau)$, where τ is a parametric time constant. This method was used for the electronic work function for all Li_xFePO_4 samples with $x \leq 0.5$. In order to obtain the electronic or ionic work function, the emission current can be plotted in an Arrhenius graph of $\ln(I_{RD} \cdot T^{-2})$ vs *1/T*.

The second method for determining work functions is photoelectron spectroscopy (PES). Conceptually, it is based on the photoelectric effect observed when shining light at a solid inducing the ejection of electrons.[44]

The electronic work function measured by photoelectron spectroscopy – in solids defined as the energetic difference between the electronic Fermi level, $E_F(e^-)$ and the vacuum level (E_{vac}) of the sample can be obtained from the difference of the excitation energy *hv* and the minimum and maximum kinetic energy (KE) of the photoelectrons obtained from the secondary electron cut-off and the Fermi level, respectively (see eqn. 4). This difference refers, on a binding energy (BE) scale, to the difference between the photon energy and the maximum observed binding energy BE_{max} and the Fermi level (BE = 0 eV). Important for such determination is the precise calibration of the Fermi level of the sample in electric contact with the ground of the spectrometer, which relies on reasonably conductive, non-charging samples. Any requirement for charge compensation by, e.g., electron or ion flooding, would compromise the precise evaluation of surface potentials and the electronic work function.

$$w(e^-) = hv - KE_{min} - KE_{max} = hv - BE_{max} - E_F(e^-) \tag{9}$$

Furthermore, the absence of any additional surface dipole potentials has to be assumed, since those would be additive to the above measured energy differences. To collect the low kinetic energy electrons efficiently, typically, a negative bias, here −3.0 V, is applied to the sample, which shifts the whole energy scale by a constant value.

As coined into the semantics, the determination of work functions by PES is restricted to electronic work functions. The photoemission of cations from a solid has not yet been demonstrated for determination of ionic work functions to our knowledge. Consequently, thermionic emission is the only established technique applicable to both electronic and ionic work function.[39] TE and PES have complementary advantages and disadvantages. The most important advantage of PES is that it does not require a specific temperature and more specifically, it is straightforwardly applied at room temperature. As a routine technique in surface physics, it is most suitable to the study of clean surfaces. Any adsorbates on the surfaces are likely to alter the measured electronic work functions. The TE presumes significantly elevated temperatures. On one hand elevated temperatures may affect the morphology and composition of a battery material, on the other hand, surface contamination is unlikely at such elevated temperatures representing an advantage of TE in this context. We finally note, that a concise introduction into the concept of work function

Research Article
doi.org/10.1002/batt.202400693
Chemistry Europe
European Chemical Societies Publishing

and what their measurement includes has been reported by Cahen and Kahn.[45]

Ultimately, in this work, the electronic and ionic work functions have been investigated for samples of the type Li_xFePO_4 and $Li_xMn_2O_4$ for several values of x, with $0 \leq x \leq 1$. All ionic work functions for the emission of lithium ions have been measured the TE. In the case of the $Li_xMn_2O_4$ samples, electronic work functions have been measured by PES. Attempts to measure the electronic work function by TE were hampered by degradation of the samples. The electronic work function for the Li_xFePO_4 samples were measured by TE. Here, attempts to measure the electronic work function by PES were hampered by charging of the surfaces during PES.

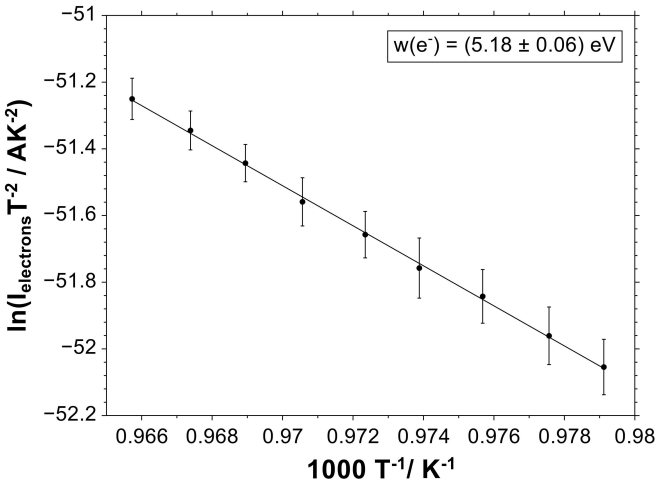

Figure 1. Richardson–Dushman plot for the emission of electrons from $Li_{0.8}FePO_4$, with the derived electronic work function.

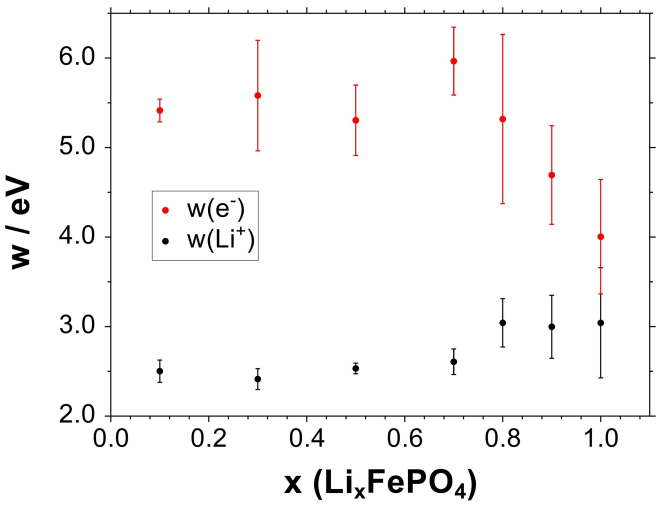

Figure 2. Ionic and electronic work functions of Li_xFePO_4 as derived from TE for different lithium concentrations x.

2. Results

2.1. Experimental Work Functions of Li_xFePO_4

The ionic and the electronic work functions of Li_xFePO_4 have been measured by the thermionic emission approach as described above in a range between $1.0 \geq x \geq 0.1$. As an example for the derivation of electronic work functions from TE measurements, Richardson-Dushman (RD) data for electron emission are shown in Figure 1.

The electronic and ionic work functions derived from such RD measurements are shown in Figure 2. We start the discussion of work functions with the fully lithiated compound ($x = 1$) and state trends in the direction of delithiation (i.e., decreasing x in Figure 2). The ionic work function determined for the fully lithiated $LiFePO_4$ state is 3.0 ± 0.6 eV. Between $1.0 \geq x \geq 0.8$ the ionic work function basically stays constant. For further on-going delithiation, i.e., $x < 0.8$ the ionic work function decreases by approximately 0.5 eV to values around 2.5 eV.

The electronic work function for fully lithiated $LiFePO_4$ is 4.0 ± 0.6 eV. With ongoing delithiation, the electronic work function markedly increases from $x = 1.0$ to $x = 0.8$ by about 1.3 eV (for uncertainties see Figure 2). For even smaller values of x the electronic work function stays around 5.3 eV. The fluctuations observed in Figure 2 for $x < 0.8$ are mostly within the experimental uncertainties. Attempts to measure the electronic work function of $LiFePO_4$ by means of PES were hampered by severe charging of the surface as shown in Figure S2 of the supplementary material.

As evident from Figure 2, the variation of the electronic work function with the state of lithiation (ca. 1.5 eV) is much more pronounced than the variation of ionic work functions (ca. 0.5 eV). There are a couple of subtle differences between the ionic and the electronic work functions. First the electronic work function increases with delithiation, while the ionic work function decreases. Second, the dominant step in the electronic work function occurs between $x = 1.0$ and $x = 0.8$, while the ionic work function only decreases at $x < 0.8$.

2.2. Experimental Work Functions of $Li_xMn_2O_4$

The ionic work function of $Li_xMn_2O_4$ has been measured by thermionic emission, the electronic work function has been measured by PES. As an example for the determination of ionic work functions, the Richardson-Dushman plot for emission of Li^+ ions from $Li_{0.76}Mn_2O_4$ is shown in Figure 3.

As an example for the derivation of electronic work functions by photoelectron spectroscopy (PES) corresponding data are shown in Figure 4. XPS survey spectra for $Li_xMn_2O_4$ with $x = 1.00$, 0.97, 0.76, 0.67 are shown in Figure S1 of the supplementary material.

The electronic and ionic work functions determined for $Li_xMn_2O_4$ are shown in Figure 5. Evidently, for this material the electronic and ionic work functions show nearly no change with the changing lithium content. All calculated ionic work functions lay in the range of 3 eV while the electronic work

Research Article
doi.org/10.1002/batt.202400693
Chemistry Europe
European Chemical Societies Publishing

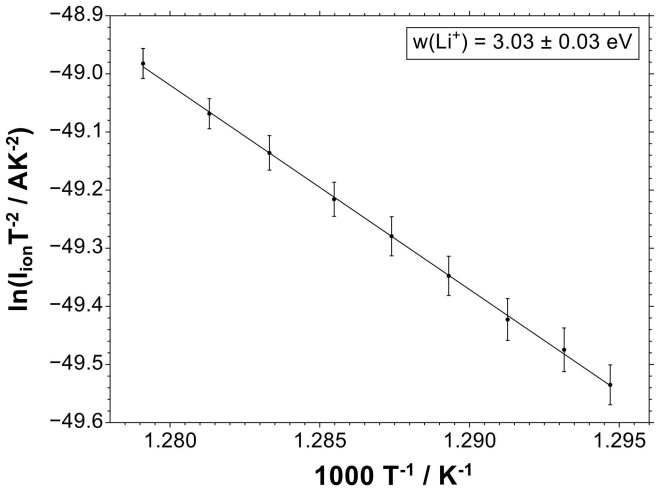

Figure 3. Richardson-Dushman plot for the emission of Li^+ ions from $Li_{0.76}Mn_2O_4$, with the ionic work function derived.

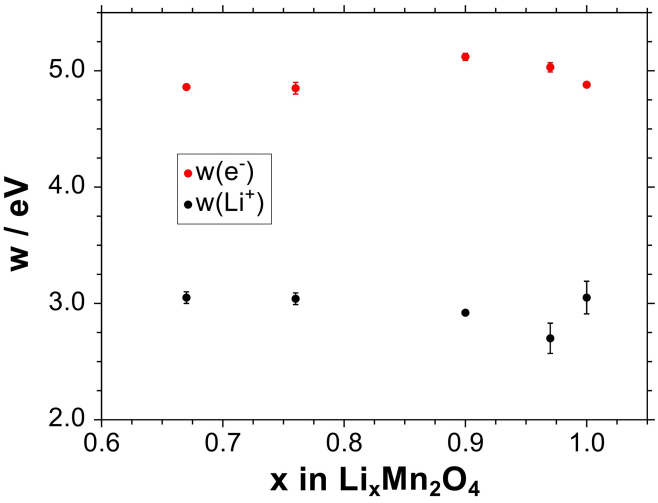

Figure 5. Ionic (TE) and electronic (PES) work functions of $Li_xMn_2O_4$ as a function of the lithium content x.

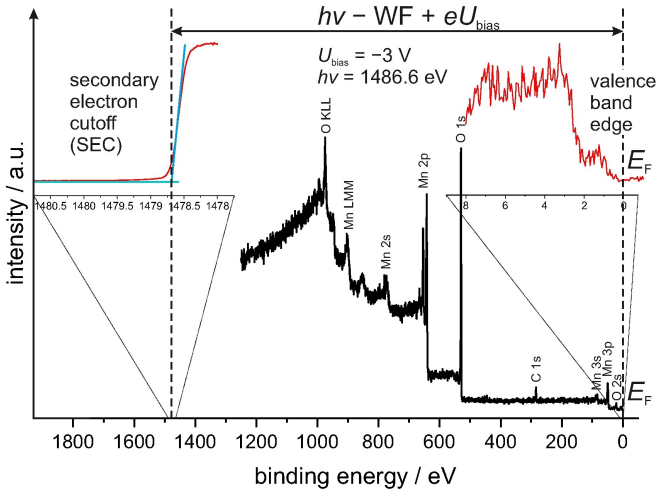

Figure 4. Exemplary PES data for $Li_{0.9}Mn_2O_4$, showing the derivation of the electronic work function. The left inset represents the secondary electron cutoff region at highest possible binding energy, i.e. kinetic energy = 0 eV. The right inset is the magnification of the valence band region of the survey spectrum showing the valence band onset (valence band maximum) and the Fermi level at 0.00 eV binding energy.

functions are all in the range of 4.9 eV to 5.1 eV. This behavior is very different from the observed variation of work functions in Li_xFePO_4, where a pronounced variation of the measured electronic work function was observed.

3. Discussion

In the following section, the work functions presented above will be discussed in the context of available literature and the prospects of better understanding thermodynamic properties of battery materials.

Structural properties of Li_xFePO_4 and $Li_xMn_2O_4$ have been extensively investigated in the past. For instance, for Li_xFePO_4, the segregation into two phase domains,[46,20] has been reported as well as the existence of solid solutions.[47] Rather little is known on the ionic or electronic work function of battery materials.[14] There appears to be a single systematic theoretical study of the electronic work function of Li_xFePO_4 as a function of the state of lithiation, x.[48] In that work, Xu et al. demonstrated that the electronic work function in Li_xFePO_4 depends on the mechanism of Li^+ extraction from the sample. This raises the question for the actual driving force of electron and ion transport, in particular, whether gradients of the particle densities or of the electrical potential dominate and whether the relevant properties (particle densities and electric fields) are homogeneous over the electrode material. There are reports on phase segregation in which case the front between two phases could propagate through the material resembling a diffusion front.[49,50,51]

All the work functions reported for the Li_xFePO_4 have been derived from thermionic emission. These data have been obtained at elevated temperatures, where the solid solution state applies. Thus, possible effects of phase segregation can be excluded in this work. Xu et al. considered two different mechanistic models for the ejection of Li^+ ions from Li_xFePO_4.[48] Model I assumes, that the surface layer is emptied of Li^+ ions first and lower layers are emptied subsequently. Model II assumes a reversed order of Li^+ ion extraction, i.e., the layers far away from the surface are emptied first and the surface layer is the last one to be emptied. Surprisingly, the work functions for model II are calculated to be lower than those for model I. Comparison between the data from Xu et al. and our data reveals a similarity in trends of model I of Xu et al. and our $w(e^-)$ measured for Li_xFePO_4. The common feature is, that primarily Li^+ ions are extracted from the near-surface regions. Possibly, the rearrangement of Li^+ ions in a transport process also plays some role. The overall similarity between our measured $w(e^-)$ and the $w(e^-)$ calculated according to model I of Xu et al. is striking.

For the $Li_xMn_2O_4$ system, again, only electronic work functions have been reported in the literature to date.

Research Article
doi.org/10.1002/batt.202400693
Chemistry Europe
European Chemical Societies Publishing

According to Qi and coworkers the electronic work function of $Li_xMn_2O_4$ does not significantly change between x = 1 and x = 0.5 – in line with the result of the current work.[52] Accidentally, the fact that $w(e^-)_{LixMn2O4}$ barely varies with a variation of x matches the characteristics reported by Xu et al. for their model II. We speculate, that the mechanism for electron emission in $Li_xMn_2O_4$ may follow model II of Xu et al.

In a study of fully lithiated $LiCoO_2$, Schuld et al. demonstrated that a Born cycle based on the electronic and ionic work function of $LiCoO_2$ was capable of rationalizing the open cell potential in a $LiCoO_2$//Li cell. Unfortunately, for the Li_xFePO_4 and the $Li_xMn_2O_4$, studied in the present work, the directly corresponding experimental data are not available in the literature. However, some important aspects can nevertheless be discussed. In a lithium ion battery, the fully lithiated cathode material corresponds to the de-charged state of the battery. The Li_xFePO_4 data presented in this work indicate that the sum of ionic and electronic work functions increases with decreasing lithium content. For $Li_xMn_2O_4$ the sum of $w(e^-)$ and $w(Li^+)$ is basically constant of the entire range of compositions studied.

As a first step towards a thermodynamic description of the electrode materials it is possible to construct Born cycles representing the open cell potential, e.g., of a Li_xFePO_4//Li and a $Li_xMn_2O_4$//Li cell, on the basis of relevant work functions. Here, we will pursue the two approaches introduced above, i.e., constructing the OCV i) based on electronic work functions only (Eq. (3)) and ii.) based on ionic and electronic work functions (Eq. (6)). While the compositional dependence of the ionic and electronic work function of Li_xFePO_4, and the $Li_xMn_2O_4$ have been measured in this work, the ionic and the electronic work function of lithium metal can be represented by single numbers as long as the lithium anode can be considered a macroscopic entity. Inserting literature data for the electronic work function of Li, $w(e^-) = 2.9$ eV,[53] and for the ionic work function of Li, $w(Li^+) = 4.122$ eV,[16] we arrive at plots of the OCV expected based on equations (3) and (6), respectively, as shown in the electronic supplementary information (Figure S3 for Li_xFePO_4 and Figure S4 for $Li_xMn_2O_4$). Also shown in Figures S3 and S4 is the respective OCV measured experimentally. Clearly, for both electrode materials the OCV expected based on Eq. (3) and Eq. (6) is significantly smaller than the measured value. The disagreement is worse for Eq. (6) compared to Eq. (3). Evidently, neither the difference of electronic work functions (Eq. (3)) nor the difference of ionic plus electronic work functions (Eq. (6)) is capable of reproducing the experimental OCV. This hints at the possibility that the models discussed so far are incomplete.

While the discussion of work functions measured in this work is based on transferring charges (ions and electrons) from a solid to the vacuum state, a realistic thermodynamic cycle applicable to battery operation has to include the transfer of charges across electrode – electrolyte interfaces and interphases. This may well become manifest, e.g., in interface/interphase potential drops due to offsets in band alignment or interface dipole formation. In particular a solid electrolyte interphase is associated with an intrinsic resistivity. By monitoring the SEI formation Gasteiger and coworkers were able to separate the resistivities connected to charge transfer from that of the SEI.[54] Interface resistivities in ion batteries are known to limit charging and decharging characteristics of ion batteries.[55] The general goal is to minimize such resistivities. In general, an interface resistance is measured in a symmetric cell, typically an electrolyte placed between two alkali metal electrodes. For a sodium battery with a NASICON electrolyte, Zhou et al.[56] reported a native interface resistance of 4000 Ohm cm^{-2}, which could be reduced by a factor of 10 by improving the electrical contact between electrode and electrolyte. For a lithium ion battery, Li et al. reported about 400 Ohm cm^{-2}.[57] The transfer of charges across such resistivities is associated with a concomitant voltage drop operative in the thermodynamic cycle describing battery operation. It is one goal of this work to stimulate further research towards a better understanding of interface and interphase properties in general and interface resistivities as a function of the composition of the cathode in particular.

Attempts to quantitatively describe the thermodynamic cycle of battery materials are also pursued by Qi and coworkers.[15,58,52] In that work the contribution of potential drops across interfaces/interphases is explicitly emphasized. Following that suggestion, we arrive at a modified Born cycle and a chemical potential balance as illustrated in Figure 6 (left). As concluded above, the OCV expected based on Eq. (6) is too small compared to experimental OCV data. Therefore, we are forced to invoke an additional interface/interphase contribution which adds to the overall Born cycle resulting in a larger OCV. Basically, the same facts can also be visualized in a chemical potential scheme as shown in Figure 6 (right), where the

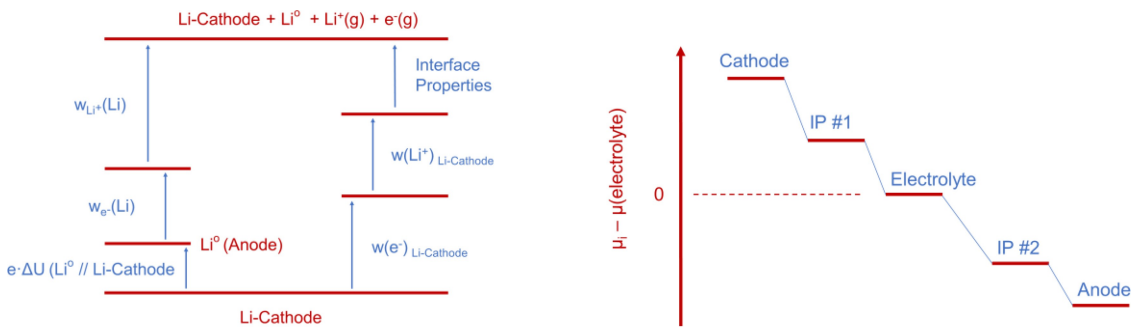

Figure 6. Born cycles for a LIB cell (left) and chemical potential scheme (right) based on contributions as discussed in the text.

chemical potential (sketched relative to that of the electrolyte) is dropping from the cathode to the anode, with contributions of two interphases, IP #1 and IP #2 as indicated. This sketch is considered to be in full analogy with the corresponding graphs by Qi and coworkers.

For better comprehension we below present some specific transport properties of the materials studied in this work. The performance of LIBs depends on the transport coefficients for the Li^+ ions, $D(Li^+)$, and the electrons, $D(e^-)$, in the materials involved, respectively.[59] Unfortunately, the numbers reported in the literature are scattered over 10 orders of magnitude for LFP. Weichert et al. reported values for $D(Li^+)$ between 10^{-12} and 10^{-11} cm^2/s.[60] Hong et al. reported 10^{-11} cm^2/s as the most likely value.[26] Sugiyama et al. reported 10^{-10} cm^2/s.[61] The theoretical value has been reported by Morgan et al. with 10^{-9} cm^2/s.[62] Yamanaga reported a value of 10^{-5} cm^2/s.[63] Most recently Šimić et al. reported significantly lower values of 10^{-15} to 10^{-13} cm^2/s.[64] All numbers refer to room temperature for the stoichiometric composition. Wang et al. reported the electronic and ionic conductivity of LFP as $4{\cdot}10^{-9}$ S/cm and $5{\cdot}10^{-5}$ S/cm[65] respectively. An electronic conductivity of $5{\cdot}10^{-9}$ S/cm has also been reported by Shi et al.[66] The intrinsically low electronic conductivity of undoped LFP can be increased significantly by appropriate doping.[67] The diffusion coefficient $D(Li^+)$ for $Li_xMn_2O_4$ has been reported to vary from 10^{-11} cm^2/s at $x=1$ to 10^{-8} cm^2/s at $x=0.5$.[68] The electronic conductivity of $LiMn_2O_4$ is on the order of 10^{-4} S/cm to 10^{-5} S/cm.[69,70]

All thermionic work function data presented in this work have been obtained at elevated temperatures around 700 K. At these temperatures the Li_xFePO_4 is usually described as a solid solution with the Li^+ ions being distributed in a $FePO_4$ network as dominated by entropy effects. At room temperature the fully lithiated $LiFePO_4$ adopts the triphylite structure as confirmed by XRD analysis. For decreasing lithium content, a superposition of different phases appears operative until at the lowest lithium content, the structure is dominated by the heterosite phase of $FePO_4$. Clearly, the structural characteristics of any real Li_xFePO_4 sample in a battery cathode will change during charging and decharging of the battery and possibly also with the number of charging cycles. The question of the correlation of ionic work functions with structural parameters has been studied by Schuld et al.[71] There, ionic work functions for alkali ion emission have been reported for alkali aluminosilicates of the spodumene type, $MAlSi_2O_6$ with M=Li, Na, K, Rb, and Cs, and the eucryptite type, $MAlSiO_4$ with M=Li, Na, K, Rb, and Cs. For most of the alkali aluminosilicates, the ionic work function was higher for the spodumene type by 0.1 eV to 0.2 eV compared to the eucryptite type, the exception being the potassium compound for which the ionic work function was higher in the eucryptite structure by 0.25 eV. Overall, the variation of ionic work functions with structural identity may be considered small. This lends support to the assumption that possible alterations in the local structure do not dominate the work functions presented in this work.

4. Conclusions

The work functions $w(Li^+)$ and $w(e^-)$, i.e., the energy required to take lithium ions and electrons out of a solid material has been investigated for two prototypical electrode materials in lithium ion batteries, Li_xFePO_4 and $Li_xMn_2O_4$. The sum of ionic and electronic work functions varies significantly with x for Li_xFePO_4 but very little for $Li_xMn_2O_4$. The variation observed for Li_xFePO_4 mainly originates from the electronic work function. Experimental measurements are based on thermionic emission and photoelectron spectroscopy. In the case of Li_xFePO_4 the electronic work function increases significantly with decreasing x, corresponding to the charging in a $Li//Li_xFePO_4$ battery, while the ionic work function decreases slightly. In the case of the $Li_xMn_2O_4$ both the ionic and the electronic work functions only mildly vary with the state of lithiation, x. This difference in the characteristic of the work function indicates a pivotal difference in the thermodynamic cycle for describing battery operation. Clearly, there is a need for more detailed theoretical calculations for e- and ion emission in such cathode materials. We again stress the advantage of considering a lithium anode in this context, because that one does not involve a concentration dependence of any property. Hopefully, the experimental demonstration of significant effects in ionic and electronic work functions stimulates such calculations. Future efforts shall be aimed at improving the understanding of complete thermodynamic cycles for ion battery operation, likely with a focus on interface/interphase properties.

Experimental Section/Methods

Synthesis: Samples of Li_xFePO_4 ($x=0.1\leq x\leq 1.0$) were obtained from $LiFePO_4$ using two different methods. For the entire range of composition, one sample was prepared by mixing of $LiFePO_4$ and $FePO_4$ with the appropriate stoichiometry as described in literature.[47] In addition to that two samples with high lithium content, i.e. $Li_{0.8}FePO_4$ and $Li_{0.9}FePO_4$, was also obtained electrochemically according to a procedure described in literature.[27] Here, Li_xFePO_4 was delithiated chemically by stirring $LiFePO_4$ (500.2 mg, 700 mg) in an aqueous solution with $K_2S_2O_8$ (107.9 mg, 299.7 mg) for (24, 188 h). The exact Li/Fe ratio of the samples was in all cases obtained using atomic emission spectrometry.

The $Li_xMn_2O_4$ samples were obtained as described in literature.[72] Li_2CO_3 and Mn_2O_3 were dried at 473 K for 5 h. Afterwards the educts were mixed with a stoichiometric Li/Mn ratio. The mixture was than heated for 12 h to 873 K and afterwards ground under acetone in an agate mortar. They were then heated to 1073 K for 24 h. The actual Li/Mn ratio of the samples was obtained using atomic emission spectrometry.

The work functions were obtained using two different methods. The ionic work functions were all obtained using thermionic emission, while the electronic work functions of the $Li_xMn_2O_4$ samples were obtained using photoelectron spectroscopy and the electronic work functions of Li_xFePO_4 using thermionic emission. The electronic work functions of $Li_xMn_2O_4$ could not be obtained using thermionic emission because the sample were not stable at the temperatures needed for this measurement. The measurement of the electronic work function of Li_xFePO_4 was not possible using

photoelectron spectroscopy as the surface showed charging effects (cf. Figure S2 of the supplementary material).

Measurement of ionic and electronic work functions by thermionic emission: The setup used in this work to determine the ionic and electronic work functions using thermionic emission was already described in earlier works.[39,73] It consists of a filament emitter, an electric lens and a tandem MCP detector. The samples were suspended in isopropanol, dropped onto the filament (a 1 mm wide ribbon of molybdenum) and finally dried. The filament can be resistively hated using heating currents up to 10 A at a potential of a few volts. The heating circuit is flowing on top of an electrostatic potential applied to the filaments. The voltages applied to the filament in this work varied between −30 V (electrons) and 10–50 V (ions). The latter covers electric fields ranging from 12.5 V/cm to 62.5 V/cm ensuring that the data fall into the Richardson-Dushman regime.[39,73] The charge carriers are accelerated towards a grounded electrostatic double mesh and afterwards detected by the tandem MCP detector. The MCP detector is operated in counting mode which allows measurements down to approximately 1×10^{-18} A. Typical currents are on the order of 10^{-16} A, implying that macroscopic depletion of the sample is negligible.

For each work function, this measurement was repeated for a minimum of eight times on each sample. The measurements were also repeated on at least one new sample. The work functions discussed here were then obtained by calculating the average over all measured work functions. For some of the electronic work functions measured for Li_xFePO_4 at smaller x a decline of the emission current with time could be observed. The time dependence of the emission current has been taken into account in the analysis.

Measurement of electronic work functions by X-ray photoelectron spectroscopy (XPS): XPS measurements were performed with monochromatic Al K_α radiation (XR 50, SPECS Surface Nano Analysis GmbH) with $h\nu = 1486.74$ eV. A hemispherical electron analyzer (PHOIBOS 150, SPECS Surface Nano Analysis GmbH) was used, calibrated with the core lines of copper (Cu 2p), silver (Ag 3d), and gold (Au 4f). Peaks were fitted using a Shirley background.[74] The powdered samples were embedded in indium foil. The In foil was covered with a sufficient amount of powder so that no indium signal from the foil was visible anymore and, thus, a contribution of the indium to the work function could be ruled out. Additionally, the amount of powder did not lead to a charging of the sample – at least for $Li_xMn_2O_4$. The secondary electron cut-off (SEC) was measured with XPS by applying a bias voltage of −3.0 V. Pass energy of the survey and detail spectra have been set to 20 eV and 10 eV, respectively.

Acknowledgements

JS and JPH acknowledge funding support from the German Federal Ministry of Education and Research BMBF under project PrometH2eus (Fkz: 03HY105H). Open Access funding enabled and organized by Projekt DEAL.

Conflict of Interests

The authors declare no conflict of interest.

Data Availability Statement

The data that support the findings of this study are available from the corresponding author upon reasonable request.

Keywords: energy storage · batteries · thermodynamic description · electronic and ionic work function · lithiation and delithiation

[1] V. Etacheri, R. Marom, R. Elazari, G. Salitra, D. Aurbach, *Energy Environ. Sci.* **2011**, *4*, 3243.
[2] S. Fang, D. Bresser, S. Passerini, *Adv. Energy Mater.* **2020**, *10*, 1902485.
[3] M. V. Reddy, G. V. Subba Rao, B. V. R. Chowdari, *Chem. Rev.* **2013**, *113*, 5364.
[4] R. van Noorden, *Nature* **2014**, *507*, 26.
[5] J. Duan, X. Tang, H. Dai, Y. Yang, W. Wu, X. Wei, Y. Huang, *Electrochem. Energy Rev.* **2020**, *3*, 1.
[6] J. B. Goodenough, K.-S. Park, *J. Am. Chem. Soc.* **2013**, *135*, 1167.
[7] L.-X. Yuan, Z.-H. Wang, W.-X. Zhang, X.-L. Hu, J.-T. Chen, Y.-H. Huang, J. B. Goodenough, *Energy Environ. Sci.* **2011**, *4*, 269.
[8] C. Liu, Z. G. Neale, G. Cao, *Mater. Today* **2016**, *19*, 109.
[9] J. Gao, S.-Q. Shi, H. Li, *Chinese Phys. B* **2016**, *25*, 18210.
[10] P. G. Bruce, *Chem. Commun.* **1997**, 1817–1824.
[11] H. Gerischer, F. Decker, B. Scrosati, *J. Electrochem. Soc.* **1994**, *141*, 2297.
[12] M. Schäfer, K.-M. Weitzel, *Materials Today Physics* **2018**, *5*, 12.
[13] M. Schäfer, D. Budina, K.-M. Weitzel, *Phys. Chem. Chem. Phys.* **2019**, *21*, 26251.
[14] S. Schuld, R. Hausbrand, M. Fingerle, W. Jaegermann, K.-M. Weitzel, *Adv. Energy Mater.* **2018**, *8*, 1703411.
[15] M. W. Swift, Y. Qi, *Phys. Rev. Lett.* **2019**, *122*, 167701.
[16] S. Li, G. S. Frankel, C. D. Taylor, *J. Electrochem. Soc.* **2022**, *169*, 81506.
[17] M. Safari, C. Delacourt, *J. Electrochem. Soc.* **2011**, *158*, A1123.
[18] A. K. Padhi, K. S. Nanjundaswamy, J. B. Goodenough, *J. Electrochem. Soc.* **1997**, *144*, 1188.
[19] Y.-H. Huang, J. B. Goodenough, *Chem. Mater.* **2008**, *20*, 7237.
[20] C. V. Ramana, A. Mauger, F. Gendron, C. M. Julien, K. Zaghib, *J. Power Sources* **2009**, *187*, 555.
[21] M. Safari, C. Delacourt, *J. Electrochem. Soc.* **2011**, *158*, A562.
[22] N. Nitta, F. Wu, J. T. Lee, G. Yushin, *Mater. Today* **2015**, *18*, 252.
[23] W.-J. Zhang, *J. Power Sources* **2011**, *196*, 2962.
[24] A. Andersson, *Solid State Ionics* **2000**, *130*, 41.
[25] J. Li, W. Yao, S. Martin, D. Vaknin, *Solid State Ionics* **2008**, *179*, 2016.
[26] L. Hong, L. Li, Y.-K. Chen-Wiegart, J. Wang, K. Xiang, L. Gan, W. Li, F. Meng, F. Wang, J. Wang, Y.-M. Chiang, S. Jin, M. Tang, *Nat. Commun.* **2017**, *8*, 1194.
[27] J. L. Dodd, R. Yazami, B. Fultz, *Electrochem. Solid-State Lett.* **2006**, *9*, A151.
[28] P. Bai, D. A. Cogswell, M. Z. Bazant, *Nano Lett.* **2011**, *11*, 4890.
[29] R. Amin, J. Maier, P. Balaya, D. P. Chen, C. T. Lin, *Solid State Ionics* **2008**, *179*, 1683.
[30] N. Ohmer, B. Fenk, D. Samuelis, C.-C. Chen, J. Maier, M. Weigand, E. Goering, G. Schütz, *Nat. Commun.* **2015**, *6*, 6045.
[31] M.-J. Lee, S. Lee, P. Oh, Y. Kim, J. Cho, *Nano Lett.* **2014**, *14*, 993.
[32] T.-F. Yi, C.-L. Hao, C.-B. Yue, R.-S. Zhu, J. Shu, *Synth. Met.* **2009**, *159*, 1255.
[33] Y. Xia, M. Yoshio, *J. Electrochem. Soc.* **1996**, *143*, 825.
[34] X. Q. Yang, *Electrochem. Solid-State Lett.* **1999**, *2*, 157.
[35] A. van der Ven, *Solid State Ionics* **2000**, *135*, 21.
[36] J. Guan, M. Liu, *Solid State Ionics* **1998**, *110*, 21.
[37] Q.-C. Zhuang, T. Wei, L.-L. Du, Y.-L. Cui, L. Fang, S.-G. Sun, *J. Phys. Chem. C* **2010**, *114*, 8614.
[38] O. W. Richardson, *The Emission of Electricity from Hot Bodies*, Longmans, Green and Company **1916**.
[39] S. Schuld, M. Diekmann, M. Schäfer, K.-M. Weitzel, *J. Appl. Phys.* **2016**, *120*, 185102.
[40] I. Langmuir, *Phys. Rev.* **1913**, *2*, 450.
[41] C. D. Child, *Phys. Rev. (Series I)* **1911**, *32*, 492.
[42] W. Schottky, *Zeitschrift für Physik* **1923**, *14*, 63.
[43] S. Dushman, *Rev. Mod. Phys.* **1930**, *2*, 381.
[44] J. W. Kim, A. Kim, *Curr. Appl. Phys.* **2021**, *31*, 52.
[45] D. Cahen, A. Kahn, *Adv. Mater.* **2003**, *15*, 271.

[46] A. Yamada, H. Koizumi, S.-I. Nishimura, N. Sonoyama, R. Kanno, M. Yonemura, T. Nakamura, Y. Kobayashi, *Nat. Mater.* **2006**, *5*, 357.
[47] C. Delacourt, P. Poizot, J.-M. Tarascon, C. Masquelier, *Nat. Mater.* **2005**, *4*, 254.
[48] G. Xu, K. Zhong, Y. Yang, J.-M. Zhang, Z. Huang, *Solid State Ionics* **2019**, *338*, 25.
[49] P. P. Prosini, *J. Electrochem. Soc.* **2005**, *152*, A1925.
[50] Y. Tian, Y. He, J. Zhang, *ECS Electrochem. Lett.* **2012**, *1*, A4–A6.
[51] P. Xiao, G. Henkelman, *ACS Nano* **2018**, *12*, 844.
[52] M. W. Swift, H. Jagad, J. Park, Y. Qie, Y. Wu, Y. Qi, *Curr. Opin. Solid State Mater. Sci.* **2022**, *26*, 100990.
[53] H. B. Michaelson, *J. Appl. Phys.* **1977**, *48*, 4729.
[54] S. Solchenbach, X. Huang, D. Pritzl, J. Landesfeind, H. A. Gasteiger, *J. Electrochem. Soc.* **2021**, *168*, 110503.
[55] H. Nara, D. Mukoyama, R. Shimizu, T. Momma, T. Osaka, *0378-7753* **2019**, *409*, 139.
[56] W. Zhou, Y. Li, S. Xin, J. B. Goodenough, *ACS Cent. Sci.* **2017**, *3*, 52.
[57] Y. Li, B. Xu, H. Xu, H. Duan, X. Lü, S. Xin, W. Zhou, L. Xue, G. Fu, A. Manthiram, J. B. Goodenough, *Angew. Chem. Int. Ed.* **2017**, *56*, 753.
[58] E. J. Fuller, E. Strelcov, J. L. Weaver, M. W. Swift, J. D. Sugar, A. Kolmakov, N. Zhitenev, J. J. McClelland, Y. Qi, J. A. Dura, A. A. Talin, *ACS Energy Lett.* **2021**, *6*, 3944.
[59] M. Park, X. Zhang, M. Chung, G. B. Less, A. M. Sastry, *J. Power Sources* **2010**, *195*, 7904.
[60] K. Weichert, W. Sigle, P. A. van Aken, J. Jamnik, C. Zhu, R. Amin, T. Acartürk, U. Starke, J. Maier, *J. Am. Chem. Soc.* **2012**, *134*, 2988.
[61] J. Sugiyama, H. Nozaki, M. Harada, K. Kamazawa, Y. Ikedo, Y. Miyake, O. Ofer, M. Månsson, E. J. Ansaldo, K. H. Chow, G. Kobayashi, R. Kanno, *Phys. Rev. B* **2012**, *85*, 54111.
[62] D. Morgan, A. van der Ven, G. Ceder, *Electrochem. Solid-State Lett.* **2004**, *7*, A30.
[63] T. Yamanaka, T. Abe, K. Nishio, Z. Ogumi, *J. Mater. Chem. A* **2018**, *6*, 11005.
[64] N. Šimić, A. Jodlbauer, M. Oberaigner, M. Nachtnebel, S. Mitsche, H. M. R. Wilkening, G. Kothleitner, W. Grogger, D. Knez, I. Hanzu, *Adv. Energy Mater.* **2024**, *14*, 2304381.
[65] C. Wang, J. Hong, *Electrochem. Solid-State Lett.* **2007**, *10*, A65.
[66] S. Shi, L. Liu, C. Ouyang, D. Wang, Z. Wang, L. Chen, X. Huang, *Physical review. B, Condensed matter* **2003**, *68*, 195108.
[67] S.-Y. Chung, J. T. Bloking, Y.-M. Chiang, *Nat. Mater.* **2002**, *1*, 123.
[68] J. Marzec, *Solid State Ionics* **2002**, *146*, 225.
[69] C. Cai, G. M. Koenig, *Electrochim. Acta* **2022**, *401*, 139484.
[70] S. Yamamura, H. Koshika, M. Nishizawa, T. Matsue, I. Uchida, *J. Solid State Electrochem.* **1998**, *2*, 211.
[71] S. Schuld, B. Harbrecht, K.-M. Weitzel, *Int. J. Mass Spectrom.* **2019**, *435*, 291.
[72] K. Raveendranath, J. Ravi, S. Jayalekshmi, T. Rasheed, K. Nair, *Mater. Sci. Eng. B* **2006**, *131*, 210.
[73] J. Schepp, D. Plamper, J. H. Both, K.-M. Weitzel, *J. Appl. Phys.* **2020**, *128*, 115108.
[74] D. A. Shirley, *Phys. Rev. B* **1972**, *5*, 4709.

Manuscript received: November 22, 2024
Accepted manuscript online: November 25, 2024
Version of record online: December 10, 2024